J. Fluid Mech. (2001), *vol.* 430, *pp.* 283–307. Printed in the United Kingdom

Experiments on Rayleigh–Bénard convection, magnetoconvection and rotating magnetoconvection in liquid gallium

By J. M. AURNOU† AND P. L. OLSON

Department of Earth and Planetary Sciences, Johns Hopkins University, Baltimore, MD 21218, USA

(Received 4 March 1999 and in revised form 12 September 2000)

Thermal convection experiments in a liquid gallium layer subject to a uniform rotation and a uniform vertical magnetic field are carried out as a function of rotation rate and magnetic field strength. Our purpose is to measure heat transfer in a low-Prandtl-number ($Pr = 0.023$), electrically conducting fluid as a function of the applied temperature difference, rotation rate, applied magnetic field strength and fluid-layer aspect ratio. For Rayleigh–Bénard (non-rotating, non-magnetic) convection we obtain a Nusselt number–Rayleigh number law $Nu = 0.129Ra^{0.272\pm0.006}$ over the range $3.0 \times 10^3 < Ra < 1.6 \times 10^4$. For non-rotating magnetoconvection, we find that the critical Rayleigh number Ra_C increases linearly with magnetic energy density, and a heat transfer law of the form $Nu \sim Ra^{1/2}$. Coherent thermal oscillations are detected in magnetoconvection at $\sim 1.4Ra_C$. For rotating magnetoconvection, we find that the convective heat transfer is inhibited by rotation, in general agreement with theoretical predictions. At low rotation rates, the critical Rayleigh number increases linearly with magnetic field intensity. At moderate rotation rates, coherent thermal oscillations are detected near the onset of convection. The oscillation frequencies are close to the frequency of rotation, indicating inertially driven, oscillatory convection. In nearly all of our experiments, no well-defined, steady convective regime is found. Instead, we detect unsteady or turbulent convection just after onset.

1. Introduction

Convection in planetary cores and stellar interiors often occurs in the presence of strong rotational and magnetic constraints. In this experimental study, we seek to understand how the effects of rotation about a vertical axis and a uniform vertical magnetic field influence thermal convection in a horizontal layer of liquid gallium that is heated from below and cooled from above.

Advances in three-dimensional numerical simulations of the geodynamo (Glatzmaier & Roberts 1997; Kuang & Bloxham 1997; Kageyama & Sato 1997; Christensen, Olson & Glatzmaier 1999) are pushing forward our knowledge of how magnetic fields are generated by convection in the Earth's metallic core and the cores of other planets. Unfortunately, the smallest Prandtl numbers that are numerically feasible are, at present, of the order of 1. As a result, the Prandtl numbers used in numerical simulations are approximately 10^2 times greater, and the magnetic Prandtl numbers are

† Present address: Department of Terrestrial Magnetism, Carnegie Institution of Washington, Washington, DC 20015, USA; e-mail: jona@dtm.ciw.edu.

Non-dimensional number	Definition	Experiment	Earth's core
Rayleigh, Ra	$\alpha g \Delta T D^3/\nu\kappa$	$< 10^5$	$> 10^{10}$
Flux Rayleigh, Ra_F	$\alpha g F D^4/\rho C_p \kappa^2 \nu$	$< 10^5$	$> 10^{10}$
Nusselt, Nu	$FD/k\Delta T$	< 2	< 10
Chandrasekhar, Q	$\sigma B^2 D^2/\rho\nu$	$< 2.6 \times 10^3$	$> 10^{10}$
Taylor, Ta	$4\Omega^2 D^4/\nu^2$	$< 10^8$	$> 10^{24}$
Prandtl, Pr	ν/κ	0.021–0.025	$\sim 10^{-2}$
Magnetic Prandtl, Pm	ν/η	1.5×10^{-6}	$\sim 10^{-8}$
Aspect Ratio, Γ	L/D	6–21	—

TABLE 1. Non-dimensional parameters in rotating magnetoconvection.

about 10^6 times greater, respectively, than those of a liquid metal. Thus, experiments using liquid metals are of great value in assessing the effects of high electrical and thermal conductivity. Here, we demonstrate how the onset of thermal convection and convective heat transfer in liquid gallium is affected by rotation and magnetic fields for Rayleigh numbers up to about 10 times critical.

The controlling non-dimensional parameters in rotating magnetoconvection are the Rayleigh number Ra, Chandrasekhar number Q, Taylor number Ta, Prandtl number Pr, and magnetic Prandtl number Pm. The Rayleigh number is the ratio of buoyancy forces to viscous forces. The Chandrasekhar number is the ratio of magnetic forces to viscous forces. The Taylor number is the squared ratio of Coriolis forces to viscous forces. In liquid gallium, both Prandtl numbers are much less than unity and Pm is much less than Pr, similar to the Earth's core. These parameters are defined in table 1. We denote the coefficient of thermal expansion by α, electrical conductivity by σ, specific heat at constant pressure by C_p, kinematic viscosity by ν, thermal diffusivity by κ and magnetic diffusivity by η. The depth of the convecting fluid layer is D and the temperature difference imposed across the layer is ΔT. The acceleration due to gravity is g, the intensity of the vertical magnetic field is B, and Ω is the angular velocity about the vertical axis. Thermal convection in bounded regions also depends on the aspect ratio of the fluid layer, $\Gamma = L/D$, where L is the horizontal dimension of the layer.

Non-dimensional heat transfer across the fluid layer is given in terms of the Nusselt number, $Nu = FD/k\Delta T$, where F is the horizontally averaged heat flux at either boundary and k is the thermal conductivity of the gallium. For purely conductive heat transfer, $Nu = 1$. When heat is also transferred across the fluid layer by convection, $Nu > 1$.

Some of the results from these experiments are expressed using the flux Rayleigh number, $Ra_F = NuRa$, also defined in table 1. The flux Rayleigh number is a non-dimensional form of the strength of the heating.

2. Previous convection studies

Most experimental studies of Rayleigh–Bénard convection (RBC) have focused on determining heat transfer laws at high-Rayleigh-number values. The early experimental studies of RBC determined a heat transfer law of the form $Nu \sim Ra^{1/3}$ at high Ra (Globe & Dropkin 1959). This power law corresponds to the regime in which the heat flux is independent of the depth of the fluid layer (Kraichnan 1962). Later RBC experiments (i.e. Heslot, Castaing & Libchaber 1987) found heat transfer laws of the

form $Nu \sim Ra^{2/7}$ for $Ra > 10^7$. Various arguments have been put forward to explain this 'hard turbulence' $2/7$ scaling exponent, based on the structure and behaviour of the boundary layers and the interaction between the boundary layers and the interior of the convecting fluid (Castaing *et al.* 1989; Shraiman & Siggia 1990; Grossman & Lohse 2000). It has also been predicted that at very high Rayleigh number (above 10^{15}–10^{20}) the heat transfer may vary as $Nu \sim (RaPr)^{1/2}$ (Kraichnan 1962). In this regime, the heat flux is insensitive to the thermal and kinematic diffusivities of the fluid, occurring when the turbulence destroys the boundary layers. Convincing evidence of this regime has yet to be found (Niemela *et al.* 2000).

In the low-Prandtl-number–moderate Rayleigh number regime relevant to the RBC experiments presented here, previous experiments indicate that the convective heat transfer first increases slowly with Ra for Rayleigh numbers just beyond critical, and then, at larger Rayleigh numbers, a more rapid increase in the convective heat transfer with Ra is observed (Chiffaudel, Fauve & Perrin 1987; Kek & Müller 1993; Horanyi, Krebs & Müller 1999). These results are in qualitative agreement with theoretical and numerical studies of steady, two-dimensional convection at low Prandtl number (Jones, Moore & Weiss 1974; Proctor 1977; Busse & Clever 1981; Clever & Busse 1981). For low-Prandtl-number convection, there is an initial regime of very weak convective heat transfer that is controlled by a balance between buoyancy and viscous forces. At higher Rayleigh numbers, these same studies find that the viscous forces are unable to balance the buoyancy forces and a new balance between inertial and buoyancy forces is established. The transition to the inertial regime is marked by a strong increase in convective heat transfer and a $Nu \sim (RaPr)^{1/4}$ power law.

Advances in computational speed and numerical methods now allow numerical simulation of three-dimensional, low-Prandtl-number RBC (Grötzbach & Wörner 1995; Verzicco & Camussi 1997, 1999). For the parameters of liquid sodium, Grötzbach & Wörner find that inertial convection occurs locally in both space and time, in regions where the large-scale flow is two-dimensional. High velocity, inertial convection leads to secondary shear instabilities at the no-slip top and bottom boundaries, similar to the experimental findings of Willis & Deardorff (1967) and Krishnamurti & Howard (1981). These shear instabilities create irregular, three-dimensional flow structures at the walls which may relate to the flow field in our experiments. Verzicco & Camussi (1999) find that their numerical results support the existence of an inertial convective regime at low Prandtl number and a hard turbulence regime at moderate Prandtl number.

Linear stability studies of magnetoconvection (MC) were first carried out by Thompson (1951) and Chandrasekhar (1961). They found that the critical Rayleigh number increases linearly with Chandrasekhar number Q in the asymptotic regime of large Q. When the magnetic Prandtl number Pm is less than the Prandtl number Pr, stationary convective onset is predicted to occur (Chandrasekhar 1961; Eltayeb 1972). In the opposite case, where the magnetic Prandtl number is greater than the Prandtl number, double diffusive magnetic instabilities can occur, producing oscillatory convective onset. For liquid gallium, $Pm \ll Pr$ and stationary convection is expected at the onset of convection.

Plane-layer MC experiments have been made by Nakagawa (1955, 1957*a*) and Jirlow (1956). In all these MC experiments, it is found that vertical magnetic fields delay the onset of thermal convection. For example, the experiments of Nakagawa (1957*a*) were carried out for Q values up to 1.65×10^5 and indicate that the critical Rayleigh number $Ra_C \sim Q$.

There is also extensive literature on the effect of rotation on convection (Nakagawa

& Frenzen 1955; Boubnov & Golitsyn 1990; Fernando, Chen & Boyer 1991; Clever & Busse 2000). Rotating convection experiments in low-Prandtl-number fluids have been made by Fultz & Nakagawa (1955), Nakagawa (1955), Dropkin & Globe (1959), Goroff (1960), and Rossby (1969). These experiments show that rotation about a vertical axis generally inhibits convective motions. This result is consistent with the restrictions implied by the Taylor–Proudman theorem, which inhibits overturning motions perpendicular to the rotation axis and thus suppresses convective heat transfer in the direction parallel to the rotation axis. In low-Prandtl-number fluids, the onset of convection occurs by overstable oscillations at sufficiently high Taylor number. Linear stability theory predicts the onset of oscillatory convection above $Ta = 10^3$ and $Ra_C \sim Ta^{2/3}$ above $Ta \sim 10^5$ for $Pr = 0.025$ (Chandrasekhar 1961).

In an analytical study of low-Prandtl number rotating convection, Zhang & Roberts (1997) find that rapidly oscillating thermal inertial waves are preferred over convective modes when $Ta \rightarrow \infty$ and $\tau = \frac{1}{2} Ta^{1/2} Pr$ remains finite. In laboratory experiments at finite Ta, it may be possible to detect thermal inertial waves when $\tau \leqslant 1$. In our experiments in gallium, $\tau \leqslant 1$ for $Ta \leqslant 10^4$. Thermal inertial waves are able to relax the Taylor–Proudman constraint through high-frequency oscillatory motion. In contrast, Chandrasekhar's convective modes are released from the Taylor–Proudman constraint by the action of viscosity at small lengthscales. In the regime where thermal inertial waves dominate convection, the critical Rayleigh number varies as $Ra_C \sim Ta^{1/4}$ (Zhang & Roberts 1997).

The literature on rotating magnetoconvection (RMC) is more limited. Nakagawa (1957*b*, 1958) determined the variation of the critical Rayleigh number in liquid mercury as a function of rotation rate and magnetic field strength. His results support the theoretical prediction by Chandrasekhar (1961) that, at large values of Taylor number and Chandrasekhar number, the critical Rayleigh number has a local minimum in the regime where $Q \sim Ta^{1/2}$. In theoretical studies, Eltayeb (1972, 1975) found that, for asymptotically large Ta and Q, the magnetic scaling law $Ra_C \sim Q$ holds when $Q \gg Ta^{1/2}$, while the rotational scaling law $Ra_C \sim Ta^{2/3}$ is followed when $Ta^{1/2} \gg Q^{3/2}$. In the range where the Lorentz and Coriolis forces are comparable, $Q < Ta^{1/2} < Q^{3/2}$, the critical Rayleigh number is reduced and varies as $Ra_C \sim Ta^{1/2} \sim Ta/Q$ (Eltayeb 1975).

In our experiments, we investigate the convective heat transfer in a plane layer of liquid gallium beyond the critical Rayleigh number. We determine how Nu varies with Ra in Rayleigh–Bénard convection (RBC) experiments, magnetoconvection (MC) experiments and rotating magnetoconvection (RMC) experiments at six values of Q. We also study the temperature–time series to determine the behaviour of the fluid layer at convective onset and in the finite-amplitude regime.

3. Experimental apparatus

The experimental apparatus consists of a convection tank and a 'magnetic capacitor' made of ceramic ferromagnets on a rotating table. Liquid gallium is used as the working fluid. The low toxicity, low vapour pressure and low melting point make gallium safer and easier to handle than mercury or liquid sodium. The physical properties of liquid gallium, including their temperature dependences, are given by Iida & Guthrie (1988) and Okada & Ozoe (1992). Nominal values of these parameters are given in table 2.

Figures 1 and 2 show the apparatus. The rectangular Lexan tank has interior dimensions of $15.2 \times 15.2 \times 3.8$ cm in height, and the walls of the Lexan tank are 1.3 cm

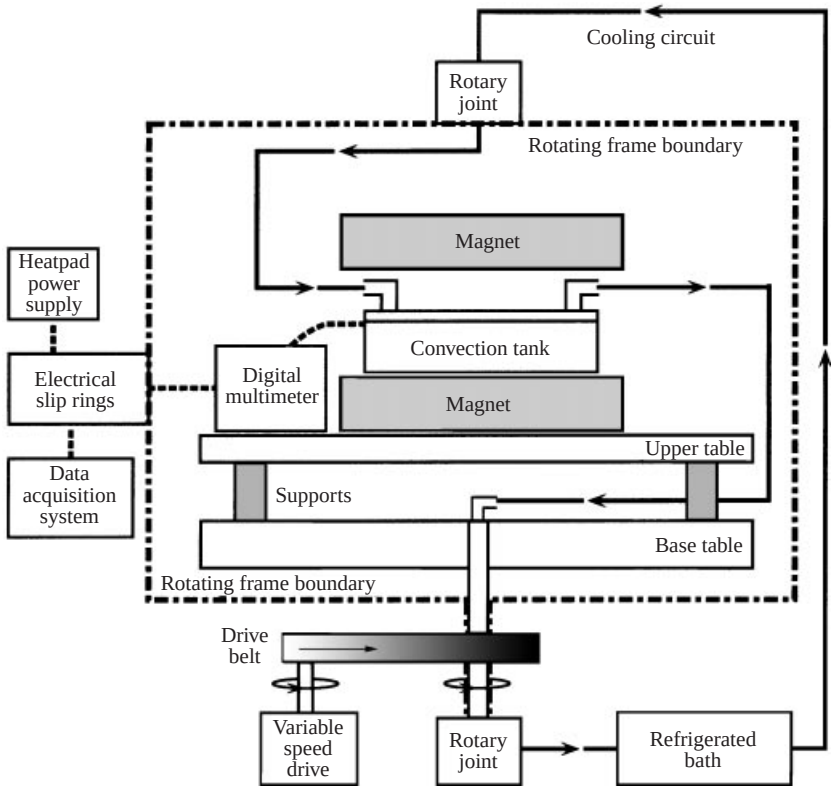

FIGURE 1. Schematic of the experimental apparatus.

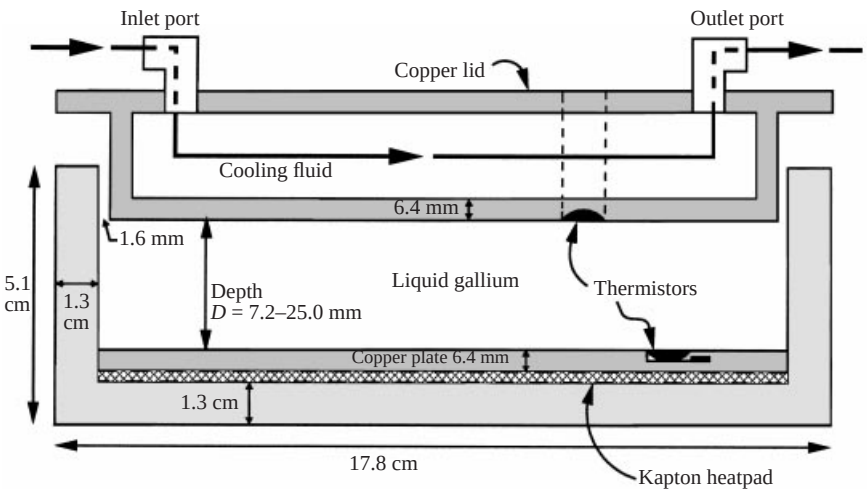

FIGURE 2. Schematic of the convection tank.

in thickness. The thermal conductivity of Lexan is 0.2 W m^{-1} K^{-1}, approximately 0.6% that of gallium. To further minimize heat losses, the convection tank is surrounded by 5 cm of foam insulation.

The depth of the liquid gallium layer was varied between 7.3 and 25 mm. The

Property	Symbol	Units	Value
Density	ρ	$\mathrm{kg\,m^{-3}}$	6.095×10^3
Density change on melting	$\Delta\rho/\rho$	—	+3.2%
Melting temperature	T_m	°C	29.7
Thermal expansion coefficient	α	$\mathrm{K^{-1}}$	1.27×10^{-4}
Specific heat	C_p	$\mathrm{J\,kg^{-1}\,K^{-1}}$	397.6
Kinematic viscosity	ν	$\mathrm{m^2\,s^{-1}}$	3.2×10^{-7}
Thermal diffusivity	κ	$\mathrm{m^2\,s^{-1}}$	1.27×10^{-5}
Thermal conductivity	k	$\mathrm{W\,m^{-1}\,K^{-1}}$	31
Magnetic diffusivity	η	$\mathrm{m^2\,s^{-1}}$	0.21
Electrical conductivity	σ	$(\mathrm{ohm\,m})^{-1}$	3.85×10^6

TABLE 2. Physical properties of liquid gallium.

majority of the convection experiments are carried out at layer depths of 18 and 25 mm, which correspond to aspect ratios $\Gamma = 8$ and 6, respectively.

Heating of the fluid layer is controlled by a Kapton resistance heating pad seated on the floor of the Lexan tank (see figure 2). The power output of the heatpad can be varied between 0 and 530 W. The heating element of the Kapton heatpad is configured such that the horizontal heating variations are less than $\pm 2\%$. The imposed heatpad power is recorded during all the experiments. The average heat flux into the fluid is calculated by dividing the heatpad power by the area of the fluid layer. Experiments in the conductive regime verify that this technique accurately determines the average value of the heat flux (see figure 5).

A 6.4 mm thick copper plate is placed on top of the Kapton heatpad. The thermal diffusivity of copper is about an order of magnitude greater than that of gallium and acts to remove spatial inhomogeneities in the heating, resulting in a nearly isothermal boundary condition. The approach to isothermal boundary conditions is estimated by the Biot number Bi, the ratio of the resistance to heat transfer in the copper plate to the resistance to heat transfer in the gallium layer,

$$Bi = \left(\frac{D_{cu}}{k_{cu}}\right) \Big/ \left(\frac{D}{k}\right) = \frac{k}{k_{cu}} \frac{D_{cu}}{D} \simeq 0.03, \tag{3.1}$$

where $D_{cu} = 6.4\,\mathrm{mm}$ and $k_{cu} = 402\,\mathrm{W\,m^{-1}\,K^{-1}}$ are the thickness and the thermal conductivity of the copper plate. For values of $Bi < 0.1$, it is found that the conductive plate is isothermal to within $\sim 5\%$ (Özişik 1980). Thus, the heating imposed at the base of the copper plate in our apparatus results in an approximately isothermal lower-thermal-boundary condition between the copper plate and the gallium.

The temperature at the upper boundary of the gallium layer is maintained by the circulation of cooling fluid through the copper lid of the convection tank (roughly 10 litres per minute). The cooling fluid, a mixture of water and ethylene glycol, is separated from the top of the gallium layer by the 6.4 mm thick bottom of the copper lid. The temperature of the cooling fluid is controlled by a refrigerated bath that is constant to within $\pm 0.05\,^\circ\mathrm{C}$.

Measurements of the temperature difference across the fluid layer are made using a single pair of YSI 700-series surface thermistors, accurate to $\pm 0.02\,\mathrm{K}$, with a resolution of $\pm 0.5\,\mathrm{mK}$. The thermistors are embedded into the top and bottom copper boundaries, one 0.5 mm above and the other 0.5 mm below the gallium layer. To avoid thermal interference with each other, the thermistors are misaligned laterally

Field intensity (gauss)	Layer depth (cm)	Chandrasekhar number, Q
121 ± 8	1.854 ± 0.003	111 ± 13
202 ± 14	1.854 ± 0.003	292 ± 42
307 ± 14	1.854 ± 0.003	669 ± 65
307 ± 14	2.500 ± 0.003	1214 ± 119
601 ± 5	1.854 ± 0.003	2562 ± 60

TABLE 3. Magnetic field intensities and corresponding Chandrasekhar numbers.

by 5 mm. A digital multimeter measures the thermistor voltages in the rotating frame and electrical slip rings pass the voltages from the multimeter to the data acquisition system in the stationary frame.

The magnetic field is generated between two parallel plates of ceramic magnets placed above and below the convection tank in the rotating frame. This arrangement produces a steady, nearly uniform, vertical magnetic field that co-rotates with the convection tank, with a maximum intensity of 601 ± 5 gauss in the region of the gallium layer. We varied the field intensity by changing the distance between the two plates, or by removing the top magnetic plate. Experiments with vertical magnetic fields are carried out at 4 different field intensities given in table 3. The errors in the vertical field intensities in table 3 refer to the spatial variations of the field measured over the volume of the gallium layer. The magnetic plates and convection tank are placed on a rotating table. The rotation rate of the table can be varied between 0.07 r.p.m. and 30 r.p.m. In calibration tests, the rotation rate remained constant to 1 part in 1000 at 5 r.p.m.

Liquid gallium presents some experimental problems because it dissolves many other metals and interacts strongly with oxygen. In our apparatus, the liquid gallium is in direct contact with copper at the upper and lower boundaries. Copper dissolves into liquid gallium with a solubility of $2.8 \times 10^{-4}\,\mathrm{g\,l^{-1}}$ at 36 °C (Zebreva & Zubtsova 1968). The small gap between the Lexan convection box and the copper lid also allows for a small region of interaction between the gallium and the atmosphere, which leads to the formation of gallium oxides. Although our apparatus produces some minor contamination of the gallium, it has the benefit of producing an effectively fully wetted contact at the upper and lower boundaries and reduces the large surface-tension forces that gallium can exert on unwetted contacts. *In situ* measurements of the thermal conductivity of the working fluid were made after the completion of the RBC experiments to verify that the bulk thermal properties correspond to pure gallium. The thermal conductivity was measured to be $k = 31.1 \pm 0.8\,\mathrm{W\,m^{-1}\,K^{-1}}$ at 35 °C, in good agreement with the values of Okada & Ozoe (1992).

The same experimental technique is used in all the RBC, MC and aspect ratio $\Gamma = 6$ RMC experiments. A fixed power is supplied to the Kapton heatpad, and the system is allowed to come to thermal equilibrium. We find that thermal equilibrium is reached after about 30 min. Temperatures are recorded for an additional 30–45 min after thermal equilibrium is reached. The power to the heatpad is then increased to begin the next experiment in the sequence, and the measurements are repeated.

Figure 3 shows the temperature difference across the gallium layer from a sequence of 9 separate RBC experiments. In the first experiment, zero power is supplied to the Kapton heatpad. In the 8 subsequent experiments, the basal heating is increased roughly once an hour to begin each new experiment in the sequence. The increase in

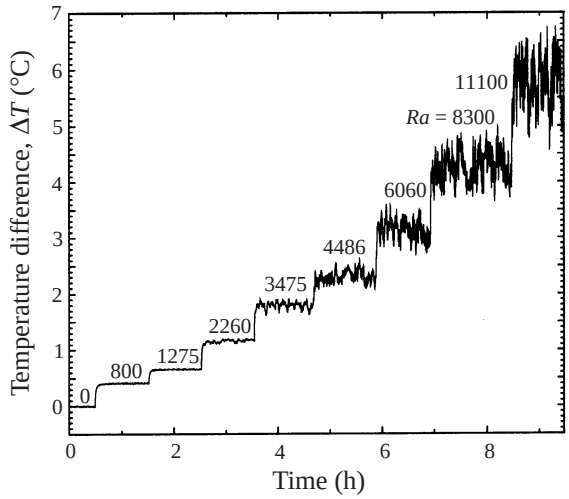

FIGURE 3. Temperature difference across the fluid layer versus time for a sequence of Rayleigh–Bénard ($Q = Ta = 0$) convection experiments in liquid gallium. Each experiment in the sequence is labelled with its average Rayleigh number.

heating causes an increase in ΔT and a corresponding increase in the value of Ra. The first three experiments in this sequence, corresponding to $Ra = 0, 800$ and 1275, are subcritical with respect to RBC. The other experiments, with Rayleigh numbers greater than 2000, are supercritical with respect to RBC. At each of the supercritical Rayleigh numbers, time-dependent fluctuations are found in the temperature records. The r.m.s. amplitude of the thermal fluctuations increases in each subsequent experiment in the sequence as the Rayleigh number is increased, implying a more strongly time-dependent convection.

A different procedure is used for the $\Gamma = 8$ RMC experiments. Here, the power to the Kapton heatpad is fixed at the same value for the entire sequence of experiments, and the rotation rate of the table is increased in a stepwise manner to begin each new experiment in the sequence. At each rotation rate, we allow 5–20 min for spin-up of the fluid layer, the exact time allowed depending upon the rotation rate. At each rotation rate, we record temperatures for 20–30 min after spin-up, in order to ensure that the convection has reached statistically stationary conditions.

The sequence of 12 experiments shown in figure 4 have a flux Rayleigh number $Ra_F = 19\,980$ and Chandrasekhar number $Q = 0$. The rotation rate of the table in the first experiment is zero. At low rotation rates, the convection is strongly time-dependent, as indicated by the large-amplitude temperature fluctuations. At higher rates of rotation the convection is suppressed, as evidenced by the decrease in the amplitude of the fluctuations. Note that the temperature difference across the fluid layer increases with rotation frequency, as proportionally more heat is transferred across the layer by conduction.

4. Rayleigh–Bénard convection (RBC) experiments

Two sets of Rayleigh–Bénard convection experiments have been made, in order to calibrate the system at subcritical Rayleigh numbers and to study low-Prandtl-number convection in gallium at supercritical-Rayleigh-number values. In the first set of experiments, the gallium layer depth is 7.26 ± 0.01 mm, corresponding to an

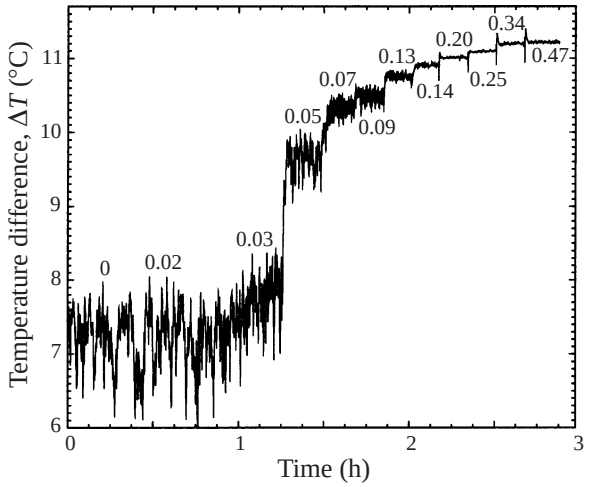

FIGURE 4. Temperature difference across the fluid layer versus time for a sequence of non-magnetic rotating convection experiments in liquid gallium. The flux Rayleigh number is held fixed at $Ra_F = 19\,980$ and the rotation rate of the table is increased to begin each new experiment in the sequence. Each experiment in the sequence is labelled with the rotation frequency (Hz) of the table.

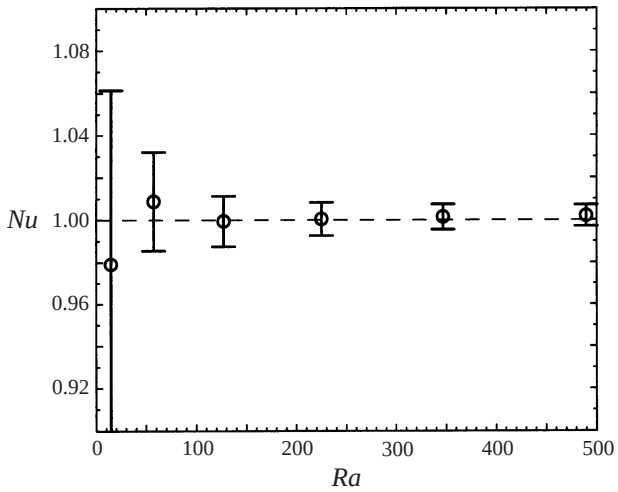

FIGURE 5. Nusselt number versus Rayleigh number for gallium in the conductive regime.

aspect ratio $\Gamma = 20.9$. The results of these experiments are shown in figure 5. For this layer depth, the maximum attainable Rayleigh number is less than 500, and the Nusselt number remains close to a value of 1.0. The errors bars plotted in figure 5 are calculated from the accuracy of the thermistors, ± 0.02 K. When the temperature difference across the fluid layer is small, the propagated errors in the value of the Nusselt numbers become large, yet the values of the Nusselt numbers remain within 5% of 1.0, even for quite low values of the Rayleigh number.

The results of experiments carried out with a layer depth of 18.31 ± 0.03 mm, corresponding to an aspect ratio $\Gamma = 8.3$, are denoted as open circles in figure 6 and solid triangles in figure 7. The maximum Rayleigh number achieved with this layer thickness is $Ra \sim 1.6 \times 10^4$. The onset of convection is located close to that predicted

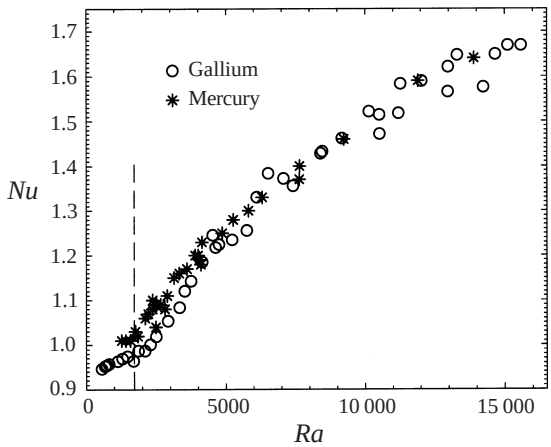

FIGURE 6. Nusselt number versus Rayleigh number for Rayleigh–Bénard convection in the range $Ra < 1.6 \times 10^4$. Nusselt numbers for liquid gallium ($Pr = 0.023$) are plotted as circles and Rossby's (1969) Nusselt numbers for mercury ($Pr = 0.024$) are plotted as stars. The dashed vertical line shows the critical Rayleigh number for an infinite layer, $Ra_C = 1708$.

by linear stability theory. A power-law fit to the Nu–Ra results yields

$$Nu = 0.129 Ra^{0.272 \pm 0.006} \quad \text{for } 2.5 \times 10^3 < Ra < 1.6 \times 10^4. \tag{4.1}$$

The intersection of this power law with a linear fit to the subcritical results yields a critical Rayleigh number of $Ra_C = 2320$.

We compare our results with Rossby (1969), who measured the Nusselt number in mercury. Rossby's Nusselt–Rayleigh results over the range of $10^3 < Ra < 1.6 \times 10^4$ are denoted by stars in figure 6. Our results in liquid gallium ($Pr \sim 0.023$) agree well with Rossby's results in mercury ($Pr \sim 0.024$) over this range of Rayleigh number, especially for $Ra > 4000$. Separate regimes corresponding to viscous and inertial convection are not evident in our Nusselt number results or Rossby's.

We use the correlation between our Nusselt results and those of Rossby (1969) to make an *in situ* calibration of our apparatus. The similarities with Rossby's results indicate that our boundary conditions are close to isothermal, and that the physical properties of the gallium are not appreciably changed by chemical interactions with the copper boundaries. For example, convection is not detected in experiments which have $Ra < 1700$ because the boundary conditions are effectively isothermal. In contrast, for a fixed temperature condition on the upper boundary and a fixed heat flux condition on the lower boundary, convection would onset at a Rayleigh number of 1296 (Sparrow, Goldstein & Johnson 1964). We also note that our agreement with Rossby's results is found in spite of major differences in the experimental geometries. Our square-sided container has an aspect ratio of 8.3 and a corresponding layer thicknesses of 18.31 mm. Rossby used cylindrical containers with aspect ratios of 32.1 and 21.6, corresponding to layer thicknesses of 6.93 mm and 10.28 mm, respectively.

Another way to estimate the critical Rayleigh number is from the r.m.s. variation of the temperature difference across the fluid layer. Figure 7(*b*) shows the r.m.s. variation of the temperature difference $\sigma_{\Delta T}$, with the RBC ($Q = 0$) results plotted as solid triangles. The value of $\sigma_{\Delta T}$ remains close to 2 mK in the conductive regime. The bifurcation of $\sigma_{\Delta T}$ provides a second estimate for the critical Rayleigh number, in this case $Ra_C = 1720$. This value is very close to 1708, the critical Rayleigh number predicted by linear theory.

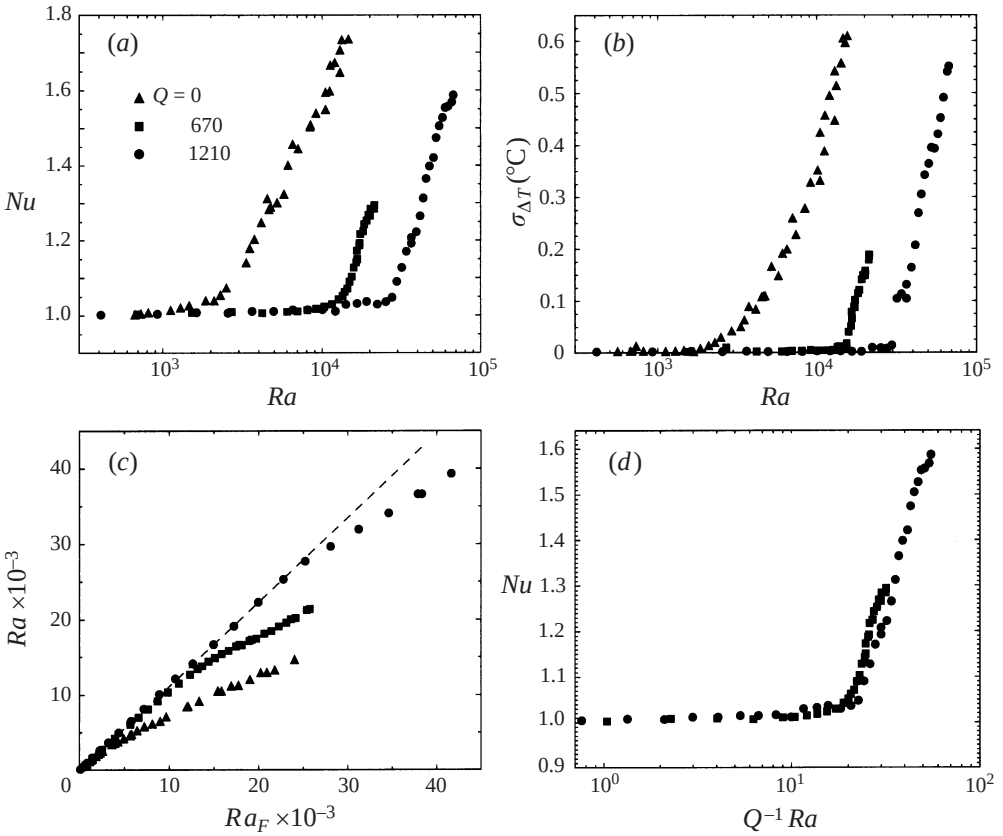

FIGURE 7. Nusselt number and temperature variation measurements in liquid gallium. ▲, Rayleigh–Bénard convection with Chandrasekhar number $Q = 0$ and aspect ratio $\Gamma = 8.3$; ■, magnetoconvection with $Q = 670$ and $\Gamma = 8.3$; ●, magnetoconvection with $Q = 1210$ and $\Gamma = 6.1$. (*a*) Nusselt number versus Rayleigh number. (*b*) The r.m.s. variation of the temperature difference measured across the fluid layer, $\sigma_{\Delta T}$, versus Rayleigh number. (*c*) Rayleigh number versus flux Rayleigh number, both reduced by 10^3. (*d*) Nusselt number versus modified Rayleigh number $Q^{-1}Ra$.

We find that time-dependent fluctuations appear in all the RBC temperature records as the first indication of the onset of convection. These irregular temperature fluctuations indicate that chaotic or even turbulent motions appear in this experiment very near to the onset of convection. Rossby (1969) and Yamanaka *et al.* (1998) also inferred the convection to be non-stationary in the supercritical regime, on the basis of irregular fluctuations in the temperature signals in mercury and liquid gallium, respectively. These inferences differ from Krishnamurti (1973), who reported steady convection in mercury over the range $1500 < Ra < 2400$, and Chiffaudel *et al.* (1987) who reported steady convection in mercury for $1700 < Ra < 2400$.

One interpretation of the irregular temperature oscillations that we observe is that they are caused by shear instabilities near the boundaries (Krishnamurti & Howard 1981; Grötzbach & Wörner 1995). The thermistors in our apparatus are shallowly embedded into the top and bottom copper boundaries, making them well-situated to detect such shear instabilities. If these oscillations are due to shear instabilities, the irregular fluctuations may not correlate with the flow field in the interior of the fluid layer. Instead, the flow field may be two-dimensional or steady far from the

Q	$Ra_C(\sigma_{\Delta T})$	$Ra_C(Nu)$	$Ra_C(Ra_F)$
0	1720	2320	2670
670	11900	12500	13500
1210	26700	27100	27300

TABLE 4. Determinations of the critical Rayleigh number Ra_C for various Chandrasekhar numbers Q from bifurcations in the curves in figure 7(*a–c*).

boundaries, especially near the onset of convection. Such a flow pattern has been reported previously by Grötzbach & Wörner (1995).

Figure 7(*c*) shows the value of the Rayleigh number versus the flux Rayleigh number. The RBC results are again plotted as solid triangles. In the conductive regime, Ra should be equal to Ra_F since the heat transfer supposedly occurs by conduction only. In the conductive regime, the experimental results define a linear trend with a slope close to 1, and the onset of convection is marked by the first deviation from this trend. By estimating the break in slope of the data for Rayleigh numbers less than 10^4, we obtain a critical Rayleigh number of $Ra_C = 2670$ for RBC.

Three different estimates of the critical Rayleigh number for RBC ($Q = 0$) and MC ($Q = 670, 1210$) are listed in table 4. Note that the critical Rayleigh number estimate produced using $\sigma_{\Delta T}$ is lower than the other two estimates for all three values of Q. We interpret this to indicate that the supercritical convection is non-stationary.

5. Magnetoconvection (MC) experiments

Two sets of magnetoconvection experiments were made with an imposed vertical magnetic field of $B = 310$ gauss. In the first set, the fluid-layer depth was 18.31 ± 0.03 mm ($\Gamma = 8$), and in the second set the depth was 25.00 ± 0.03 mm ($\Gamma = 6$), equivalent to Chandrasekhar numbers of $Q = 670$ and 1210, respectively. Figure 7 shows the results from these experiments, along with the $Q = 0$ results (RBC). For increasing values of Q, the onset of convection, marked by the bifurcations in figure 7(*a–c*), occurs at higher Rayleigh numbers (see table 4). This has been observed previously in magnetoconvection experiments by Nakagawa (1955, 1957*a*), Jirlow (1956) and Lehnert & Little (1957). Figure 7(*d*) shows the Nusselt number versus the modified Rayleigh number $Q^{-1}Ra$, from our experiments. Note that the $Q = 670$ and $Q = 1210$ Nusselt number results have the same behaviour when plotted this way. We find that for large Q, the critical Rayleigh number scales as $Ra_C \sim Q$, in agreement with the results of Nakagawa (1957*a*).

Our Nusselt numbers in the supercritical magnetoconvection regime, that is, for $Q^{-1}Ra > 25$, fit the following power laws:

$$Nu = 0.23(Q^{-1}Ra)^{0.50\pm0.03} \quad \text{for } Q = 670, \tag{5.1}$$

$$Nu = 0.23(Q^{-1}Ra)^{0.49\pm0.02} \quad \text{for } Q = 1210. \tag{5.2}$$

The $Nu \propto (Q^{-1}Ra)^{1/2}$ power law can be derived from simple scaling considerations. Assuming the basic force balance is between buoyancy and the Lorentz force gives

$$g\alpha\Delta T \sim \frac{\sigma u B^2}{\rho}, \tag{5.3}$$

where u is the characteristic convective velocity. Similarly, the heat equation balance

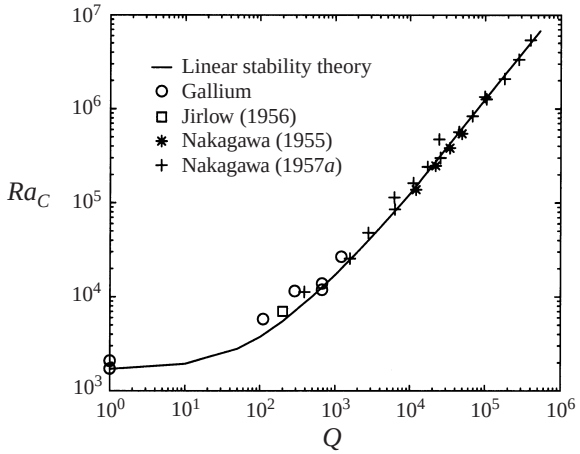

FIGURE 8. Critical Rayleigh numbers versus Chandrasekhar numbers obtained from magnetoconvection experiments.

is between advection and boundary-layer conduction, which implies

$$u\frac{\Delta T}{D} \sim \kappa\frac{\Delta T}{\delta^2}, \tag{5.4}$$

where δ is the thickness of the thermal boundary layer. Combining (5.3) and (5.4) yields

$$\frac{\rho g\alpha\Delta T}{\sigma B^2 D} \sim \frac{\kappa}{\delta^2}. \tag{5.5}$$

This relationship is equivalent to

$$Nu \sim (Q^{-1}Ra)^{1/2}. \tag{5.6}$$

We find that the Nusselt number in the MC experiments increases as $Ra^{1/2}$ in the supercritical regime, in comparison to $Ra^{0.27}$ for RBC. Assuming both these power laws continue to hold at higher Rayleigh-number values, then the two curves will intersect at some Ra, and at some still larger Ra, the Nusselt number will be greater for MC than for RBC. This suggests that the presence of the vertical magnetic field can actually increase the efficiency of the convective heat transfer at sufficiently high values of the Rayleigh number, an effect seen in the numerical calculations by Clever & Busse (1989). Combining (4.1) with (5.1) and (5.2), we find this intersection occurs at $Ra \sim 1.3 \times 10^5$ for $Q = 670$ and $Ra \sim 4.6 \times 10^5$ for $Q = 1210$, respectively. The $Nu \sim Ra^{1/2}$ regime must eventually break down for sufficiently large Ra. Further experiments are required to determine under what conditions this regime breaks down and whether situations exist where vertical magnetic fields increase the efficiency of MC relative to RBC.

Figure 8 shows our determinations of the critical Rayleigh number versus the Chandrasekhar number for MC. The solid line represents the critical Rayleigh number for stationary convection obtained from linear stability theory (Chandrasekhar 1961). Our critical Rayleigh numbers found in gallium are marked by open circles. Three of the circles correspond to the critical Rayleigh numbers determined in figure 7(*b*) at $Q = 0$, 670 and 1210. The others correspond to critical Rayleigh numbers determined from the $\Gamma = 8$ RMC Nusselt number results with $Ta < 2.5 \times 10^3$. The open square is from Jirlow (1956) for MC in mercury. The star and plus symbols denote MC results

in mercury from Nakagawa (1955) and Nakagawa (1957*a*), respectively. The $Q = 0$ and $Q = 670$ critical Rayleigh numbers determined from $\sigma_{\Delta T}$ in figure 7(*b*) agree very closely with the results of linear stability theory. The four critical Rayleigh numbers determined from the Nusselt number bifurcation in the $\Gamma = 8$ RMC experiments are all greater than the values predicted by linear stability theory. Note that the results for $Q = 0, 110$ and 290 exceed the values predicted from linear theory by roughly 10–15%. This discrepancy lies within the uncertainty of our experiments and may not be significant.

Coherent thermal oscillations are detected in our MC experiments in the finite-amplitude regime, but are not observed at the onset of convection. This agrees with the results of linear stability theory, which predict that the onset of convection is stationary in low-Prandtl-number fluids. Here, we are interpreting the irregular thermal oscillations that mark the onset of convection as turbulent boundary structures caused by local shear instabilities. The irregular oscillations may not require large-scale oscillatory convection to be occurring throughout the fluid layer. The frequency of the coherent thermal oscillations are 0.022 Hz in $\Gamma = 6$, $Q = 1210$ magnetoconvection experiments at $Ra = 1.4Ra_C$. The frequency of the oscillations is too small to be caused by Alfvén waves. For the parameter values in these experiments, the Alfvén wave frequency is close to 2 Hz, roughly two orders of magnitude greater than the frequency we detect.

In all our RBC and MC experiments with fluid aspect ratios of 8 or less, we find that Nu lies between 0.93 and 1.0 in the conductive regime (see figure 6). We interpret Nu-values systematically less than 1.0 in the conductive regime to be a consequence of the finite value of the aspect ratio of the tank. The results shown in figures 5 and 6 demonstrate that Nu is very close to 1.0 in the conductive regime when the gallium layer aspect ratio is of the order of 20, whereas Nu values becomes less than 1.0 when the aspect ratio is less than 10. In order to correct for this effect in the power-law fits and figures, we normalize our Nusselt values such that the lowest value in the subcritical regime equals 1. An increase in Nu with increasing Ra is also apparent in the conductive regime in figure 6. This is probably caused by subcritical motions occurring in the fluid layer. Subcritical motions in liquid metals can be driven by very small lateral temperature gradients along the upper boundary, for example.

6. Rotating magnetoconvection (RMC) experiments

In RMC experiments, we find the Nusselt number monotonically decreases and the critical Rayleigh number monotonically increases with increasing Chandrasekhar and Taylor numbers. This result contrasts with Nakagawa (1957*b*, 1958), who found local minima in the critical Rayleigh number in the region $Q \sim Ta^{1/2}$, although for much higher values of Ra, Q and Ta than in our experiments.

6.1. *Aspect ratio 8 rotating magnetoconvection*

Figure 9 shows contour fits of the Nusselt number as a function of the Taylor and Rayleigh numbers for $\Gamma = 8$. The four plots in figure 9 correspond to experiments with Chandrasekhar numbers of 0, 110, 290 and 670, respectively. Contours with Nusselt numbers greater than 1.06 are drawn as solid lines and contours for Nusselt numbers less than 1.06 are drawn with dashed lines. This has been done to estimate where the subcritical (dashed lines) and supercritical regimes are located. The '+' symbols denote the location of the experiments in each plot.

The Nusselt number decreases for Taylor numbers above 10^4, in response to the

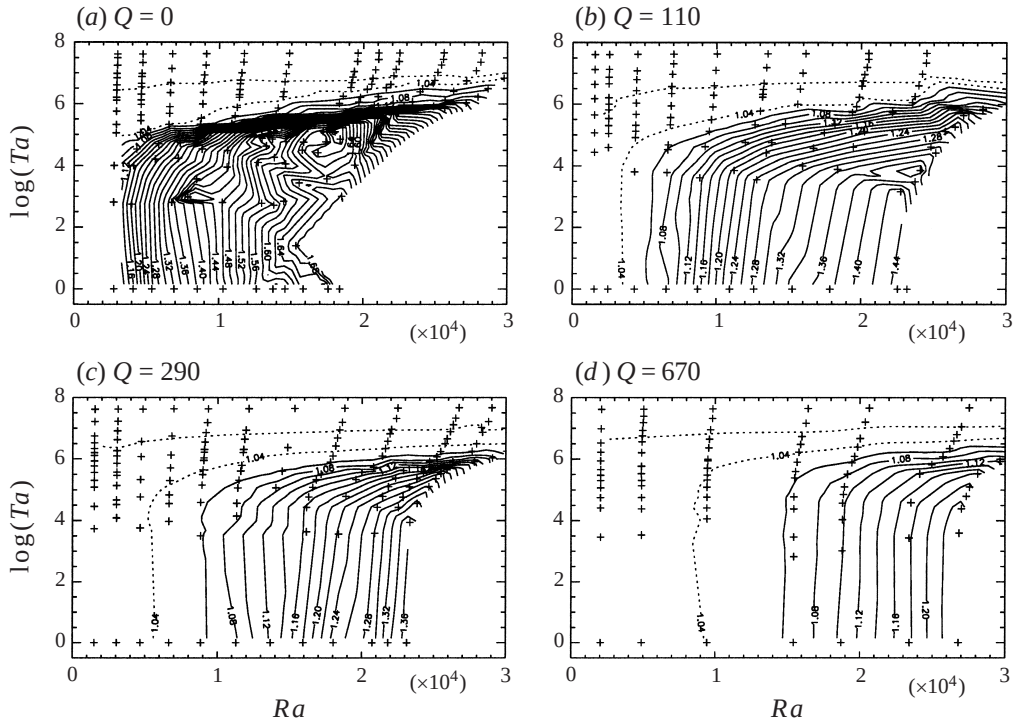

FIGURE 9. Contour plots of Nusselt number versus Taylor number and Rayleigh number for aspect ratio $\Gamma = 8$ rotating magnetoconvection in liquid gallium. (*a*) Rotating non-magnetic convection ($Q = 0$). (*b–d*) Rotating magnetoconvection for different Q-values. The contour interval is 0.02 in each case. The contours are drawn as solid lines for $Nu \geqslant 1.06$, to denote the convective regime. Dashed contours are used for $Nu < 1.06$ to represent the conductive regime. +, locations of experimental data points.

stabilizing effect of the rotation. For Taylor numbers less than 10^4, Nu is not strongly affected by rotation. The $Q = 0$ (rotating convection) experiments in figure 9(*a*) clearly demonstrate that convection is strongly inhibited for $Ta > 10^5$, in agreement with linear stability theory (Chandrasekhar 1961).

The results in figure 9 indicate that the vertical magnetic field delays the onset of convection and reduces the value of the Nusselt number, relative to non-magnetic convection. The value of Ra_C is close to 2400 for $Q = 0$. For $Q = 110$, $Ra_C = 5850$; for $Q = 290$, $Ra_C = 1.15 \times 10^4$; for $Q = 670$, $Ra_C = 1.38 \times 10^4$. Here, we estimate the critical Rayleigh number using the bifurcation in the r.m.s. variation of the temperature difference across the fluid layer, $\sigma_{\Delta T}$. At the highest magnetic field strength $Q = 2560$, convection does not occur over the range of Rayleigh numbers studied.

Figure 10 shows profiles of slices through the contour surfaces of figure 9. Figures 10(*a*) and 10(*b*) show slices of Nu versus $\log_{10} Ta$ for two different Ra-values. Figures 10(*c*) and 10(*d*) show slices of Nu versus Ra for different fixed Ta-values. In figure 10(*a*), the Rayleigh number is 5000 and the Nusselt number is supercritical in the $Q = 0$ case for $Ta < 1.6 \times 10^5$. The Nusselt number is weakly supercritical for $Q = 110$ and is subcritical in the other Q-cases. In figure 10(*b*), the Rayleigh number is 17 300 and the Nusselt number remains supercritical in the $Q = 0$ case up to $Ta = 2.0 \times 10^6$. The Taylor number is 1.4×10^5 in figure 10(*c*) and convection occurs above $Ra = 4100$ for $Q = 0$. In figure 10(*d*), the Taylor number is 3.3×10^5 and

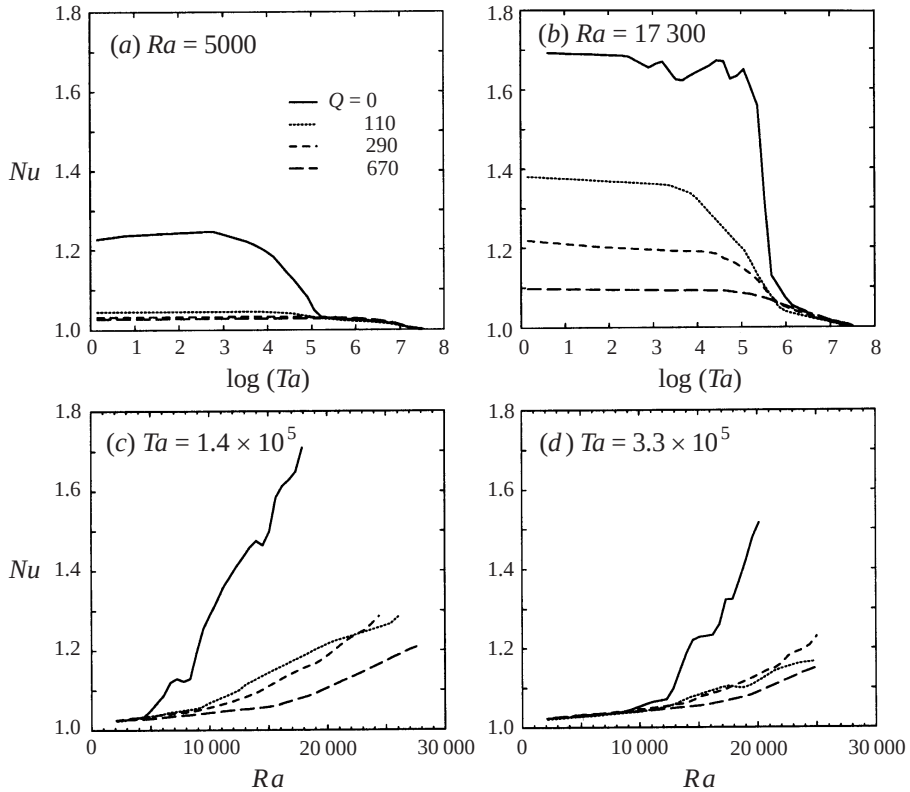

FIGURE 10. (a, b) Nusselt number versus Taylor number at fixed Rayleigh number for aspect ratio $\Gamma = 8$ rotating magnetoconvection in liquid gallium. (c, d) Nusselt number versus Rayleigh number at fixed Taylor number for the same experiments.

convection occurs above $Ra = 8900$ for the $Q = 0$ case. Note that the Nusselt number increases with a weaker functional dependence on the Rayleigh number for $Q = 110$, 290, 670 RMC compared to the $Q = 0$ case in figures 10(c) and 10(d). This differs from the $Q = 670, 1210$ MC experiments where we find that the Nusselt number increases more sharply with the vertical magnetic field present.

In figure 11, $\Gamma = 8$ RMC Nusselt numbers are contoured in terms of a modified Rayleigh number $Q^{-1/2}Ra$. Before contouring, the data has been smoothed using a two-dimensional five-point stencil. The onset of convection occurs at $Q^{-1/2}Ra \sim 530$. Comparing figure 11 with figure 7 reveals a significant difference. For MC, the Nusselt number scales with $Q^{-1}Ra$. In contrast, figure 11 shows that Nu scales with $Q^{-1/2}Ra$ for RMC.

6.2. *Aspect ratio 6 rotating magnetoconvection*

RMC experiments have also been made with a layer depth of 25 mm and an imposed magnetic field of 310 gauss, corresponding to $\Gamma = 6$ and $Q = 1210$, respectively. The results of experiments with this aspect ratio are systematic but qualitatively different from those found in the $\Gamma = 8$ RMC experiments described above. Here, the Taylor number is held constant and the Rayleigh number is varied in the general manner shown in figure 3. Measurements were made for six different values of Ta, ranging from $0 < Ta < 5 \times 10^6$ (see table 5). For this aspect ratio, the maximum Rayleigh number attained is nearly 10^5.

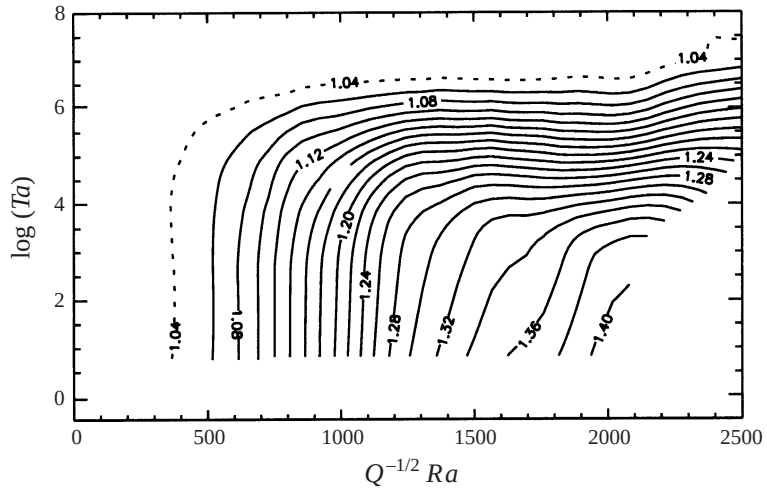

FIGURE 11. Smoothed contour fit to all the aspect ratio $\Gamma = 8$ rotating magnetoconvection Nusselt numbers shown in figure 9, as a function of Taylor number and modified Rayleigh number $Q^{-1/2}Ra$.

Ta	$Ra_C(\sigma_{\Delta T})$	$Ra_C(Nu)$	$Ra_C(Ra_F)$
0	26 700	27 100	27 300
9.7×10^2	29 300	25 500	25 300
1.1×10^4	28 300	28 300	27 600
9.5×10^4	30 000	29 800	29 800
1.0×10^6	47 100	44 500	45 300
5.2×10^6	83 700	79 900	—

TABLE 5. Determinations of the critical Rayleigh number Ra_C at $Q = 1210$ for various Ta values. The results shown in figures 12(*a*) to 12(*c*) are used in determining Ra_C.

Figure 12(*a*) shows the Nusselt number versus the Rayleigh number for six different Taylor number values. Figure 12(*b*) shows $\sigma_{\Delta T}$ as a function of the Rayleigh number. Figure 12(*c*) shows the Rayleigh number versus the flux Rayleigh number. Figure 12(*d*) shows a contour fit of the Nusselt number as a function of Taylor and Rayleigh numbers for $\Gamma = 6$ and $Q = 1210$. Bifurcations in the curves in figures 12(*a*) to 12(*c*) yield the critical Rayleigh number estimates given in table 5. The onset of convection is detected first from bifurcations in the Nu–Ra and Ra_F–Ra curves in the cases with $Ta > 0$. We infer that the onset of convection is stationary only in these cases.

The results in figure 12 and table 5 indicate that the onset of convection is determined by the ratio $Q/Ta^{1/2}$, in general agreement with Chandrasekhar (1961) and Eltayeb (1972, 1975). In the regime where $Q > Ta^{1/2}$, the Lorentz force is greater than the Coriolis force and the onset of convection is controlled by the magnetic field. In cases where $Q < Ta^{1/2}$, the Coriolis force is greater than the Lorentz force and the onset of convection is controlled by rotation. At $Q = 1210$, the Lorentz force is greater than the Coriolis forces when the Taylor number is less than 1.5×10^6. In these experiments the critical Rayleigh number sharply increases owing to rotation above $Ta = 10^6$. In contrast, when $Ta < 10^6$, the convection is dominated by the Lorentz force so the critical Rayleigh number depends on Q and is independent of Ta. For example, the linear stability theory of Eltayeb (1972) predicts that in the double

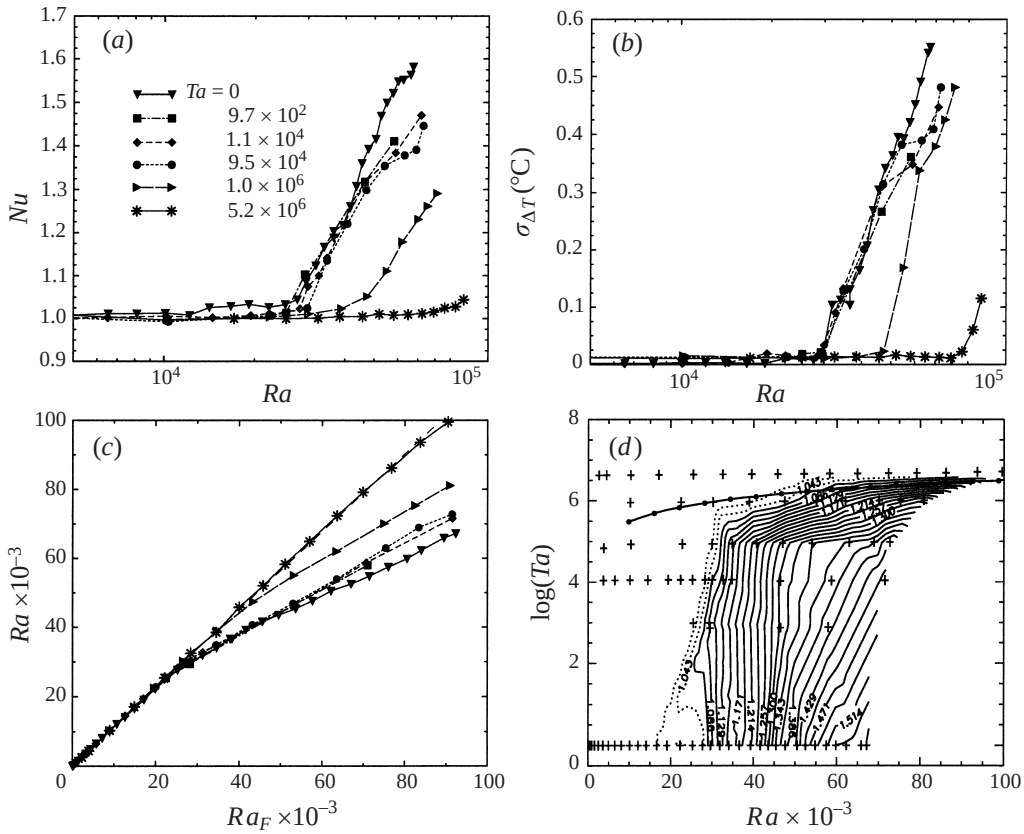

FIGURE 12. Results of rotating magnetoconvection experiments with $Q = 1210$ and $\Gamma = 6$. (*a*) Nusselt number versus Rayleigh number at various Taylor numbers. (*b*) The r.m.s. variation of the temperature difference across the fluid layer versus Rayleigh number. (*c*) Rayleigh number versus flux Rayleigh number. (*d*) Contour fit of Nusselt number as a function of Taylor number and Rayleigh number, similar to figure 9. The circles connected by the solid line denote Ra_C values from the asymptotic scaling law of Eltayeb (1972) in the regime where Lorentz and Coriolis forces are comparable.

asymptotic limit of large Ta and Q, the critical Rayleigh number for stationary convection scales as $Ra_C \sim 39.5Ta/Q$ over the range $0.5Q < Ta^{1/2} < 0.1Q^{3/2}$ for rigid, electrically insulating boundaries. For $Q = 1210$, this corresponds to the range of Taylor numbers between 3.7×10^5 and 1.8×10^7. Critical Rayleigh numbers predicted by this scaling law are plotted in figure 12(*d*) for comparison with our experimental results. Above $Ta \sim 10^6$, the asymptotic law agrees well with our results.

7. Thermal oscillations and oscillatory convection

Coherent thermal oscillations are detected in our experiments in two different situations. High-frequency coherent oscillations are found in $\Gamma = 8$ non-magnetic rotating convection experiments at frequencies close to the inertial frequency, when $Ta > 10^5$. Also, lower-frequency coherent thermal oscillations are found in the $\Gamma = 6$, $Q = 1210$ RMC experiments at low-Taylor-number values, where $Ta^{1/2} < Q$. The high-frequency inertial oscillations exist in the regime where the Coriolis force controls

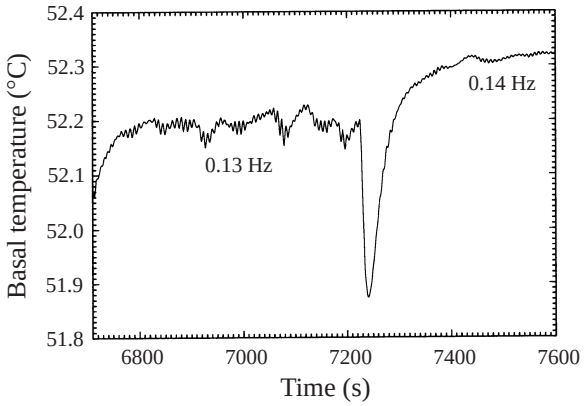

FIGURE 13. Inertially driven thermal oscillations recorded in the basal thermistor at $Ra_F = 19\,980$, $Q = 0$ and $Ta \sim 3.3 \times 10^6$, taken from the experimental sequence shown in figure 4.

the convection. The low-frequency oscillations are found where the Lorentz force controls the convection.

Figure 13 shows an example of the high-frequency temperature oscillations detected in $\Gamma = 8$ rotating convection. These temperature signals were recorded on the thermistor located at the base of the gallium layer during two successive experiments at $Ra_F = 19\,980$, the first with a rotation frequency of 0.13 Hz and the second with a rotation frequency of 0.14 Hz. The corresponding values of the Taylor number are 3.1×10^6 and 3.5×10^6, respectively. The amplitude and frequency of the oscillations vary with the rotation frequency. The large downward spike is an artefact, due to EMFs induced in the electrical slip rings when the rotation rate of the table is changed between experiments.

Figure 14 shows temperature spectral density versus frequency from experiments at $Ra_F = 13\,100$. Individual spectra are identified by their Taylor numbers and associated rotation frequencies. The broad peaks observed in the $Ta = 4.4 \times 10^5$, 6.6×10^5 and 1.6×10^6 temperature spectra correspond to inertially driven thermal oscillations. For example, the lowest-frequency oscillations in figure 14 have a frequency $f = 0.067$ Hz at $Ta = 4.4 \times 10^5$, corresponding to a non-dimensional frequency $f/2\Omega = 0.69$. Exact thermal inertial wave calculations (Zhang & Roberts 1997) have been made for comparison with our results assuming $Ta = 4.4 \times 10^5$ and rigid, isothermal boundary conditions (K. Zhang, personal communication). These calculations predict $f/2\Omega = 0.64$ at $Ra_C = 4.3 \times 10^3$. Thus, the experimental and theoretically predicted oscillation frequencies are similar.

Note that oscillations are absent in the $Ta = 1.1 \times 10^5$ spectrum in figure 14(*a*). At this relatively low Ta value, the convection is far beyond the critical Rayleigh number. Here, coherent oscillations in the fluid are replaced by less regular motions. Oscillations are also absent in the $Ta = 3.9 \times 10^7$ spectrum, but for a different reason. In this case, the Rayleigh number is subcritical for convection. The spectra in figure 14 that do show peaks are found in the range $4 \times 10^5 < Ta < 2 \times 10^6$. Inertially driven thermal oscillations are detected in this range because the layer is unstable to convection, and is also strongly influenced by the rotation. Rotating experiments have also been performed without heating, to determine if these oscillations were erroneously produced by the temperature-measurement system. In these tests, coherent thermal oscillations are not observed over the full range of rotation rates examined.

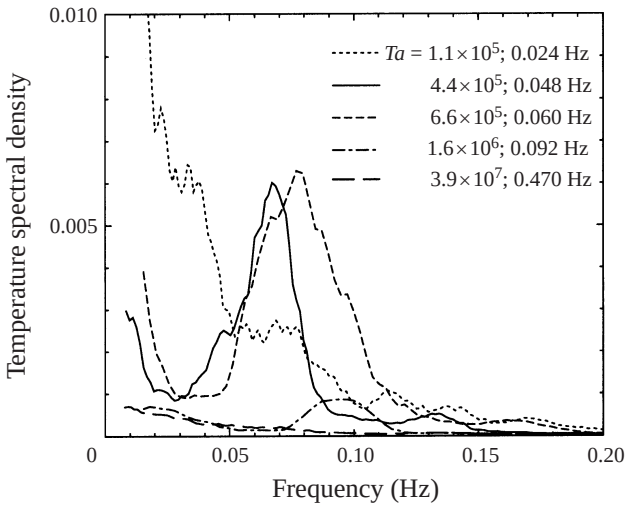

FIGURE 14. Temperature spectra from rotating non-magnetic convection experiments in liquid gallium at $Ra_F = 13\,100$.

Non-dimensional oscillation frequencies, $f/2\Omega$, measured in several of the non-magnetic rotating convection experiments are plotted in figure 15. Oscillations from experiments at four different values of Ra_F are shown. Thermal oscillations are measured over a range of rotation rates for a given value of the flux Rayleigh number (see figure 14). At each value of Ra_F, the oscillations detected at the highest Taylor numbers correspond to the value of Nu closest to 1.0 and, therefore, occur closest to convective onset. The solid line in figure 15 denotes Chandrasekhar's (1961) theoretical oscillation frequencies at the onset of convection for $P = 0.025$ and stress free boundaries.

Figure 16 shows the critical Rayleigh numbers in the $Ta^{1/2} > Q$ regime. These critical Rayleigh numbers are determined from the breaks in slope of Nusselt number versus Taylor number using plots similar to figures 10(a) and 10(b) and the results given in table 5. For example, in figure 10(b), convection ceases in the $Q = 110$ case above a Taylor number $Ta = 10^6$. Critical Rayleigh numbers in figure 16 are located between $Ta = 1.5 \times 10^5$ and $Ta = 7.4 \times 10^6$. The solid line in figure 16 shows critical Rayleigh numbers for oscillatory convection obtained from Chandrasekhar's (1961) linear stability analysis of non-magnetic rotating convection, the long-dashed line corresponds to the critical Rayleigh numbers for steady onset (Chandrasekhar 1961) and the short-dashed line shows the $Ra_C \propto Ta^{1/4}$ trend predicted by Zhang & Roberts (1997) for thermal inertial waves in the asymptotic limit. The majority of the results are located close to the critical Rayleigh numbers for oscillatory convection. This supports our interpretation that the convective onset occurs as oscillatory convection in our RMC experiments with $Ta > 10^5$ and $Ta^{1/2} > Q$. Our present results are not at sufficiently high values of Ta to test the validity of the $Ra_C \sim Ta^{2/3}$ asymptotic scaling laws of Chandrasekhar (1961) or the $Ra_C \sim Ta^{1/4}$ scaling law of Zhang & Roberts (1997).

Low-frequency, magnetically-controlled coherent thermal oscillations are detected in the $\Gamma = 6$, $Q = 1210$ RMC experiments (see figure 17). These oscillations are observed in the range $Ra = 1.1Ra_C$ to $1.4Ra_C$ in experiments between $Ta = 0$ and $Ta = 9.5 \times 10^4$ such that $Ta^{1/2}/Q < \frac{1}{4}$, corresponding to the low-Taylor-number

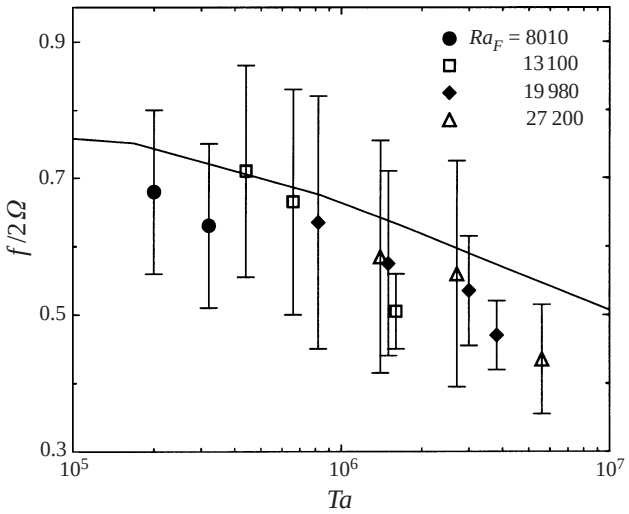

FIGURE 15. Thermal oscillation frequency normalized by the inertial frequency, $f/2\Omega$, versus Taylor number for rotating convection in liquid gallium at various values of flux Rayleigh number. The solid line represents the predicted oscillation frequency at the onset of convection when both boundaries are stress free (Chandrasekhar 1961). The error bars denote the uncertainty in the oscillation frequencies.

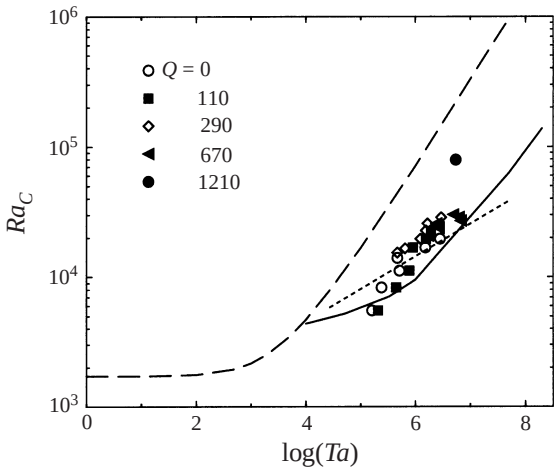

FIGURE 16. Critical Rayleigh number versus Taylor number for rotating magnetoconvection in gallium. The long-dashed line denotes the critical Rayleigh number for oscillatory convection predicted by linear stability theory and the solid line denotes the critical Rayleigh number for steady convection (Chandrasekhar 1961). The short-dashed line shows an $Ra_C \sim Ta^{1/4}$ scaling law predicted for thermal inertial waves in the asymptotic regime (Zhang & Roberts 1997).

regime. The oscillation frequencies are given in table 6. These frequencies are roughly an order of magnitude lower than those of the inertially driven oscillations shown in figure 14.

In table 6, the non-dimensional oscillation frequency is defined as fD^2/κ, where $D = 2.5\,\text{cm}$ and $\kappa = 1.27 \times 10^{-5}\,\text{m}^2\,\text{s}^{-1}$. The non-dimensionalized oscillation frequencies are close to 1 for magnetoconvection at $Ra/Ra_C = 1.4$. In the rotating magnetoconvection experiments at $Ta = 1.1 \times 10^4$ and 9.5×10^4, the primary spectral peak again

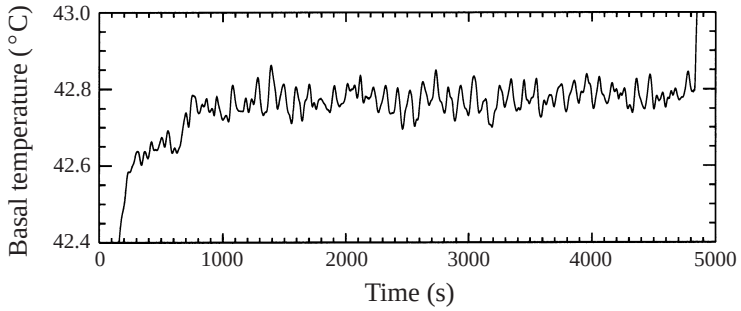

FIGURE 17. Thermal oscillations recorded in the basal thermistor at $Ra = 3.04 \times 10^4$, $Q = 1210$ and $Ta \sim 1.1 \times 10^4$.

Ra/Ra_C	Ra	Ta	f (Hz)	fD^2/κ
1.37	3.66×10^4	0	0.021	1.02
1.39	3.71×10^4	0	0.022	1.07
1.10	3.04×10^4	1.1×10^4	0.010, 0.019	0.48, 0.92
1.18	3.27×10^4	1.1×10^4	0.010, 0.020	0.48, 0.97
1.26	3.47×10^4	1.1×10^4	0.011, 0.022	0.53, 1.07
1.17	3.49×10^4	9.5×10^4	0.013, 0.026	0.63, 1.26

TABLE 6. Coherent thermal oscillation frequencies and non-dimensionalized frequencies in $\Gamma = 6$, $Q = 1210$ magnetoconvection and rotating magnetoconvection experiments.

corresponds to a non-dimensional frequency close to 1. However, a secondary spectral peak is also detected with a non-dimensional frequency value of ~ 0.5. The primary oscillation frequency is roughly a factor of 2 larger than Busse & Clever's (1996) non-dimensional frequency estimate at $Q = 1000$ for oscillating knot convection. The secondary oscillation frequency agrees well with their numerical results. In their numerical study of nonlinear magnetoconvection, Busse & Clever (1996) assume a spatially periodic planform and calculate the oscillation frequency at the transition from steady knot convection to oscillating knot convection. In comparing our results, it should be noted that the convective planform in our experiments is probably not spatially periodic or steady.

8. Summary

We have measured the Nusselt number and the temperature variations in thermal convection in a layer of liquid gallium subject to the combined action of vertical rotation and a uniform vertical magnetic field. We find that the vertical magnetic field and rotation each individually inhibit the onset of convection. The simultaneous action of both forces also tends to inhibit the convection, in the sense that we measure a reduction in convective heat transfer when both are present. Our key results are summarized in table 7. For Rayleigh–Bénard convection we find a heat transfer law of the form $Nu \sim Ra^{0.272}$. For non-rotating magnetoconvection, we find a heat transfer law of the form $Nu \sim (Q^{-1}Ra)^{1/2}$. We find that rotating magnetoconvection is controlled by a modified Rayleigh number $Q^{-1/2}Ra$ over the regime $Ra < 3 \times 10^4$ and $Q \leqslant 670$.

This contrasts with the results of Nakagawa (1957*a*), who found the modified

Experiment	Result	Range
RBC, MC, $\Gamma = 8$ RMC	Non-stationary onset	All experiments
$\Gamma = 6$ RMC	Stationary onset	$Q = 1210$; $10^3 < Ta < 5 \times 10^6$
RBC	$Nu = 0.129Ra^{0.272}$	$2.5 \times 10^3 < Ra < 1.6 \times 10^4$
MC	$Ra_C \sim Q$	$Q = 670, 1210$
MC	$Nu = 0.23(Q^{-1}Ra)^{1/2}$	$25 < Q^{-1}Ra < 60$; $Q = 670, 1210$
$\Gamma = 8$ RMC	$Ra_C \sim Q^{1/2}$	$Ra < 3 \times 10^4$; $Q \leqslant 670$
MC	0.02 Hz coherent oscillations	$Q = 1210$; $Ra/Ra_C \sim 1.4$
$\Gamma = 6$ RMC	0.01–0.02 Hz coherent oscillations	$Q = 1210$; $10^4 < Ta < 10^5$; $1.1 \sim Ra/Ra_C \sim 1.3$
$\Gamma = 8$ RMC	O (0.1 Hz) inertial oscillations	$Q = 0$; $Ta > 10^5$

TABLE 7. Summary of key experimental results. RBC = Rayleigh–Bénard convection, MC = magnetoconvection, RMC = rotating magnetoconvection.

Rayleigh number to be $Q^{-1}Ra$, but at higher Ra and Q-values. We observe that, at sufficiently high Taylor number, convection is rotationally inhibited. The convection ceases in all the experiments for which the Taylor number is increased above the critical value predicted for the onset of oscillatory rotating convection. Inertial thermal oscillations are measured in the aspect ratio $\Gamma = 8$ rotating convection experiments. The oscillation frequency f is proportional to the inertial frequency 2Ω and their ratio $f/2\Omega$ decreases with increasing Taylor number. Low-frequency oscillations are detected in the supercritical regime magnetoconvection experiments, in qualitative agreement with predictions by Busse & Clever (1996). The critical Rayleigh numbers determined at high Ta values agree well with critical Rayleigh numbers obtained from linear stability theory for oscillatory, rotating convection, even though we do not detect the thermal oscillations that linear stability theory predicts at the onset of convection.

We also find that the onset of convection coincides with the detection of irregular temperature fluctuations in nearly all cases. Only in exceptional cases did we observe stationary convection, even at slightly supercritical Rayleigh numbers. In fact, we do not find any regime where the convection appears to be entirely stationary. Instead, we find evidence for unsteady or perhaps turbulent convection just beyond the critical Rayleigh number in liquid gallium.

We thank Brendan Meade for designing the data acquisition software, Keke Zhang for providing the thermal inertial wave calculation, Tom Rossby for his experimental results in mercury, and three anonymous referees. This research was supported by the National Science Foundation Geophysics Program.

REFERENCES

BOUBNOV, B. M. & GOLITSYN, G. S. 1990 Temperature and velocity field regimes of convective motions in a rotating plane fluid layer. *J. Fluid Mech.* **219**, 215–239.

BUSSE, F. H. & CLEVER, R. M. 1981 An asymptotic model of two-dimensional convection in the limit of low Prandtl number. *J. Fluid Mech.* **102**, 75–83.

BUSSE, F. H. & CLEVER, R. M. 1996 Three-dimensional convection in the presence of a strong vertical magnetic field. *Eur. J. Mech.* B **15**, 1–15.

Castaing, B., Gunaratne, G., Heslot, F., Kadanoff, L., Libchaber, A., Thomae, S.,Wu, X., Zaleski, S. & Zanetti, G. 1989 Scaling of hard thermal turbulence in Rayleigh–Bénard convection. *J. Fluid Mech.* **204**, 1–30.

Chandrasekhar, S. 1961 *Hydrodynamic and Hydromagnetic Stability*. Clarendon.

Chiffaudel, A., Fauve, S. & Perrin, B. 1987 Viscous and inertial convection at low Prandtl number: experimental study. *Europhys. Lett.* **4**, 555–560.

Christensen, U., Olson, P. & Glatzmaier, G. A. 1999 Numerical modelling of the geodynamo: a systematic parameter study. *Geophys. J. Intl* **138**, 393–409.

Clever, R. M. & Busse, F. H. 1981 Low Prandtl number convection in a layer heated from below. *J. Fluid Mech.* **102**, 61–74.

Clever, R. M. & Busse, F. H. 1989 Nonlinear oscillatory convection in the presence of a vertical magnetic field. *J. Fluid Mech.* **201**, 507–523.

Clever, R. M. & Busse, F. H. 2000 Convection in a low Prandtl number fluid layer rotating about a vertical axis. *Eur. J. Mech.* B **19**, 213–227.

Dropkin, D. & Globe, S. 1959 Effect of spin on natural convection in mercury heated from below. *J. Appl. Phys.* **30**, 84–89.

Eltayeb, I. A. 1972 Hydromagnetic convection in a rapidly rotating fluid layer. *Proc. R. Soc. Lond.* A **326**, 229–254.

Eltayeb, I. A. 1975 Overstable hydromagnetic convection in a rotating fluid layer. *J. Fluid Mech.* **71**, 161–179.

Fernando, H. J. S., Chen, R.-R. & Boyer, D. L. 1991 Effects of rotation on convective turbulence. *J. Fluid Mech.* **228**, 513–547.

Fultz, D. & Nakagawa, Y. 1955 Experiments on over-stable thermal convection in mercury. *Proc. R. Soc. Lond.* A **231**, 211–225.

Glatzmaier, G. A. & Roberts, P. H. 1997 Simulating the geodynamo. *Contemp. Phys.* **38**, 269–288.

Globe, S. & Dropkin, D. 1959 Natural-convection heat transfer in liquids confined by two horizontal plates and heated from below. *Trans. ASME* C: *J. Heat Transfer* February, 24–28.

Goroff, I. R. 1960 An experiment on heat transfer by over-stable and ordinary convection. *Proc. R. Soc. Lond.* A **254**, 537–541.

Grossman, S. & Lohse, D. 2000 Scaling in thermal convection: a unifying theory. *J. Fluid Mech.* **407**, 27–56.

Grötzbach, G. & Wörner, M. 1995 Inertial convection in turbulent Rayleigh–Bénard convection at small Prandtl numbers. In *Computational Fluid Dynamics: Selected Topics* (ed. D. Leutloff & R. C. Srivastava). Springer.

Heslot, F., Castaing, B. & Libchaber, A. 1987 Transitions to turbulence in helium gas. *Phys. Rev.* A **36**, 5870–5873.

Horanyi, S., Krebs, L. & Müller, U. 1999 Turbulent Rayleigh–Bénard convection in low Prandtl number fluids. *Intl J. Heat Mass Transfer* **42**, 3983–4003.

Iida, T. & Guthrie, R. 1988 *The Physical Properties of Liquid Metals*. Clarendon.

Jirlow, K. 1956 Experimental investigation of the inhibition of convection by a magnetic field. *Tellus* **8**, 252–253.

Jones, C. A., Moore, D. R. & Weiss, N. O. 1976 Axisymmetric convection in a cylinder. *J. Fluid Mech.* **73**, 353–388.

Kageyama, A. & Sato, T. 1997 Velocity and magnetic field structures in a magnetohydromagnetic dynamo. *Phys. Plasmas* **4**, 1569–1575.

Kek, V. & Müller, U. 1993 Low Prandtl number convection in layers heated from below. *Intl J. Heat Mass Transfer* **36**, 2795–2804.

Kraichnan, R. 1962 Turbulent thermal convection at arbitrary Prandtl number. *Phys. Fluids* **5**, 1374–1389.

Krishnamurti, R. 1973 Some further studies on the transition to turbulent convection. *J. Fluid Mech.* **60**, 285–303.

Krishnamurti, R. & Howard, L. N. 1981 Large-scale flow generation in turbulent convection. *Proc. Natl Acad. Sci. USA* **78**, 1981–1985.

Kuang, W. & Bloxham, J. 1997 An Earth-like numerical dynamo model. *Nature* **389**, 371–374.

Lehnert, B. & Little, N. C. 1957 Experiments on the effect of inhomogeneity and obliquity of a magnetic field in inhibiting convection. *Tellus* **9**, 97–103.

NAKAGAWA, Y. 1955 An experiment on the inhibition of thermal convection by a magnetic field. *Proc. R. Soc. Lond.* A **175**, 417–419.

NAKAGAWA, Y. 1957*a* Experiments on the inhibition of thermal convection by a magnetic field. *Proc. R. Soc. Lond.* A **240**, 108–113.

NAKAGAWA, Y. 1957*b* Experiments on the instability of a layer of mercury heated from below and subject to the simultaneous action of a magnetic field and rotation. *Proc. R. Soc. Lond.* A **242**, 81–88.

NAKAGAWA, Y. 1958 Experiments on the instability of a layer of mercury heated from below and subject to the simultaneous action of a magnetic field and rotation. II. *Proc. R. Soc. Lond.* A **249**, 138–145.

NAKAGAWA, Y. & FRENZEN, P. 1955 A theoretical and experimental study of cellular convection in rotating fluids. *Tellus* **7**, 1–21.

NIEMELA, J. J., SKRBEK, L., SREENIVASAN, K. R. & DONNELLY, R. J. 2000 Turbulent convection at very high Rayleigh numbers. *Nature* **404**, 837–840.

OKADA, K. & OZOE, H. 1992 Experimental heat transfer rates of natural convection of molten gallium suppressed under an external magnetic field in either the x, y, or z direction. *J. Heat Transfer* **114**, 107–114.

ÖZIŞIK, M. N. 1980 *Heat Conduction.* John Wiley.

PROCTOR, M. R. E. 1977 Inertial convection at low Prandtl number. *J. Fluid Mech.* **82**, 97–114.

ROSSBY, H. T. 1969 A study of Bénard convection with and without rotation. *J. Fluid Mech.* **36**, 309–335.

SHRAIMAN, B. I. & SIGGIA, E. D. 1990 Heat transport in high-Rayleigh-number convection. *Phys. Rev.* A **42**, 3650–3653.

SIGGIA, E. 1994 High Rayleigh number convection. *Ann. Rev. Fluid Mech.* **26**, 137–168.

SPARROW, E. M., GOLDSTEIN, R. J. & JOHNSON, V. H. 1964 Thermal instability in a horizontal fluid layer: effect of boundary conditions and nonlinear temperature profile. *J. Fluid Mech.* **18**, 513–528.

THOMPSON, W. 1951 Thermal convection in a magnetic field. *Phil. Mag.* **42**, 1417–1432.

VERZICCO, R. & CAMUSSI, R. 1997 Transitional regimes of low-Prandtl thermal convection in a cylindrical cell. *Phys. Fluids* **9**, 1287–1295.

VERZICCO, R. & CAMUSSI, R. 1999 Prandtl number effects in convective turbulence. *J. Fluid Mech.* **383**, 55–73.

WILLIS, G. E. & DEARDORFF, J. W. 1967 Development of short-period temperature fluctuations in thermal convection. *Phys. Fluids* **5**, 931–937.

YAMANAKA, Y., KAKIMOTO, K., OZOE, H. & CHURCHILL, S. 1998 Rayleigh–Bénard oscillatory natural convection of liquid gallium heated from below. *Chem. Engng J.* **71**, 201–205.

ZEBREVA, A. I. & ZUBTSOVA, R. A. 1968 Electrochemical properties of the gallium electrode. V. Determination of the solubility of copper in gallium by a polarographic method. *Izv. Vyssh. Ucheb. Zaved., Khim. Khim. Tekhnol.* **11**, 921–4.

ZHANG, K. & ROBERTS, P. R. 1997 Thermal inertial waves in a rotating fluid layer: Exact and asymptotic solutions. *Phys. Fluids* **9**, 1980–1987.